Prospects for electrically pumped organic lasers

M. A. Baldo,* R. J. Holmes, and S. R. Forrest
Center for Photonics and Optoelectronic Materials (POEM), Department of Electrical Engineering and the Princeton Materials Institute, Princeton University, Princeton, New Jersey 08544

(Received 18 October 2001; revised manuscript received 7 March 2002; published 19 July 2002)

We examine the effects of nonradiative losses on lasing in crystalline and amorphous organic thin films. In crystalline films, the dominant loss mechanism is singlet-singlet annihilation, and this must be avoided if lasing is to be achieved at practical current densities. The electrically pumped crystalline-tetracene laser structure of Schön *et al.* [Science **289**, 599 (2000)] is studied in detail. Optical and electrical confinement in the bulk structure appears unable to explain the spectral narrowing reported; consequently, we consider electron-hole plasmas, self-focusing at interfaces, and crystal defects as possible sources of the reported phenomena. In amorphous films, lasers are likely to have to operate at current densities $J<1000$ A/cm^2 due to a combination of nonradiative losses. The performance of potential lasing materials is quantified by the external quantum efficiency-current–density product, $\eta_{EXT}J$. Electrically pumped lasers require $\eta_{EXT}J\sim 5$ A/cm^2; the best amorphous devices currently posses $\eta_{EXT}J\sim 0.3$ A/cm^2. However, we demonstrate that electrically pumped lasing in amorphous materials should be possible using indirect pumping techniques.

DOI: 10.1103/PhysRevB.66.035321 PACS number(s): 78.45.+h, 42.60.By, 42.70.Hj, 42.70.Jk

I. INTRODUCTION

Recent reports of electrically pumped lasing and optical gain in organic semiconductor crystals,[1,2] and optically pumped lasing in amorphous semiconducting thin films[3–8] have encouraged the pursuit of practical organic semiconductor lasers. Organic thin films accommodate low-cost fabrication, and can exploit the wide variety of dye molecules in inexpensive plastic lasers tunable across the visible spectrum.[9] These properties may ultimately enable organic materials to find practical application in electrically pumped lasers. But despite the achievement of stimulated emission using optically pumped amorphous organic thin films,[3–8] electrical pumping has not, to date, proven successful in achieving gain or lasing.[10,11]

Conventional semiconductor lasers use covalently bonded crystalline materials. One reason for the success of these devices is that the photoluminescence efficiency of a direct-energy-gap crystalline semiconductor such as GaAs is $\approx$100%, independent of excitation strength.[12] Organic light-emitting devices (OLED's) have also demonstrated[13] a maximum internal efficiency approaching 100%. However, the highest-efficiency organic electroluminescence is typically realized at low current densities because nonradiative losses increase at higher biases. At the excitation densities required for electrically pumped lasing, such losses might render organic lasers impractical.

Previously, the inability to realize electrically pumped lasers using amorphous organic films was attributed to the optical absorption of injected charge, or "polaron absorption."[10,14–16] In this work we examine singlet-singlet, singlet-polaron, and singlet-triplet quenching, and electric-field-induced exciton dissociation. Singlet-singlet annihilation may prevent the achievement of lasing in crystalline materials, unless it can be overcome. In amorphous films that employ Förster energy transfer between host and guest molecules,[3,8] singlet-polaron quenching limits the quantum efficiency. The effect of all nonradiative processes is quantified by the external quantum efficiency-current density product, $\eta_{EXT}J$. Since singlet-polaron quenching is the nonradiative analog of polaron absorption, an intensity-independent quantum efficiency is associated with low polaron absorption. Bimolecular nonradiative losses such as singlet-polaron annihilation increase with excitation strength, thus amorphous thin-film laser structures must be designed to operate at threshold current densities $J_{TH}<1000$ A/cm^2.

As a prototype crystalline laser, the tetracene device of Schön *et al.*[1] is studied in detail. Although electrically pumped lasing has not been convincingly demonstrated, the significant spectral narrowing reported in Ref. 1 suggests that lasing may be achievable with a slightly improved device structure. The bulk tetracene crystals used in this device possess low optical confinement, making it difficult to account for the observation of spectral narrowing at the reported threshold current density. Consequently, we investigate the possible effects of electron-hole plasmas (EHP's) and defect or interface initiated self-focusing. We find that the formation of an EHP may replace the dominance of excitonic effects in the optical properties of organic semiconductors with more bandlike characteristics. This, in turn, reduces or even eliminates multiexciton annihilation, which presents a significant barrier to gain at lower excitation densities.

This paper is organized as follows: in Secs. II A and II B, current and field dependent nonradiative losses are analyzed, respectively; in Sec. III, the lasing threshold in organic materials is calculated in terms of a quantum efficiency-current density product; nonradiative losses in amorphous materials are studied in Sec. IV A; the tetracene device of Schön *et al.*[1] is studied in Sec. IV B; we discuss self-focusing and electron-hole plasmas in organic materials and the relative advantages of crystalline and amorphous materials in Sec. V, and conclude in Sec. VI.

II. NONRADIATIVE LOSSES IN ORGANIC MATERIALS

A. Current-density dependent limitations to electrically pumped lasing

Energy transfer to singlet excitons, triplet excitons, and polarons is an ubiquitous source of loss in organic materials.[17] For losses to occur, it is necessary for the absorption spectrum of the quenching species to overlap with the fluorescence spectrum of the radiative singlet exciton. The energy of the singlet exciton may then be transferred to the quenching species, either by long-range Förster transfer or by a direct collision-mediated exchange. It is possible, for example, that singlet fluorescence in an organic molecule will overlap with the polaron absorption spectrum. Owing to the increased electrical polarization of a charged molecule and its neighbors, the optical transitions of the ionized species are typically redshifted with respect to those of the neutral molecule.[17] Therefore, in systems where Förster energy transfer[18] from host to guest molecules is prevalent, guest polarons are likely to cause quenching of host singlets (see Sec. IV A). Similarly, the transition between the first and second triplet excited states is typically less than the energy of the first singlet excited state.[19] Thus, exchange energy interactions ensure that singlet fluorescence in an organic molecule will overlap with its triplet absorption.

As current density increases, these losses also increase and are consequently expected to be significant in electrically pumped lasers. The rate of energy-transfer-mediated singlet-exciton quenching is[17]

$$\kappa = 4\pi DR, \tag{1}$$

where D is the diffusion constant of singlet excitons and R is the energy-transfer radius, dependent on the overlap of the singlet emission spectrum with the absorption spectrum of the quenching species.[18] Here, κ represents nonradiative rates that depend on the concentration of the quenching species. For nonradiative rates that are not empirically determined, an energy-transfer radius of $R \sim 10$ Å is often assumed.[17]

Equation (1) suggests that nonradiative losses are especially severe in crystalline materials, because the diffusion constant of singlet excitons, D, increases with molecular order.[20] Indeed, energy transfer between singlet excitons is a significant loss mechanism in crystalline materials such as tetracene, where the singlet diffusion constant is estimated to be $D \sim 4\times10^{-2}$ cm^2/s,[17] as compared to $D \sim 1\times10^{-5}$ cm^2/s in an amorphous material such as tris(8-hydroxyquinoline) aluminum (Alq_3).[21] This process, known as singlet-singlet annihilation, follows:

$$S^* + S^* \xrightarrow{\kappa_{SS}} S^* + S, \tag{2}$$

where the rate is κ_{SS}, and S^* and S are the excited and ground molecular singlet states, respectively.

Although singlet-singlet annihilation is much stronger in crystalline than in amorphous materials, singlet-triplet and singlet-polaron losses are typically weaker. Consequently, in crystalline laser structures such as that of Schön *et al.*[1] shown in Fig. 1(a), we concentrate our analysis on singlet-singlet annihilation. Molecular order in crystals increases the charge transport mobility, which lowers the density of polarons at a given current density and increases the rate of triplet losses, decreasing singlet-triplet annihilation. Tetracene has rates of triplet-triplet and triplet-polaron annihilation that are at least two orders of magnitude higher than in naphthalene, anthracene, or pyrene,[17] and the resultant reduction in triplet density makes tetracene particularly well suited among crystalline materials for lasing. Band transport in crystalline materials further reduces singlet-triplet and singlet-polaron losses at low temperature, whereas field and thermally assisted hopping in amorphous materials freezes out triplet diffusion and retards charge transport as the temperature is decreased.

To calculate nonradiative losses in amorphous materials using Eq. (1), it is necessary to estimate the concentration of polarons and triplets within an electrically pumped device. The free charge within most undoped organic materials is negligible. Hence, current flow requires the injection of charge, and in the absence of injection barriers and charge traps, the current is space-charge limited,[22] i.e., $J = \frac{9}{8}\mu\varepsilon V^2/d^3$, where d is the film thickness, μ is the charge transport mobility, and ε is the permittivity. In this case, the space-charge density is

$$n = \left(\frac{J\varepsilon}{2\mu d q^2}\right)^{1/2}. \tag{3}$$

Equation (3) relates the minimum density of absorptive polarons (n) within an organic film to the charge transport mobility.

Although Eq. (3) gives the fundamental limit for a trap-free semiconducting organic film, OLED's are often electron-injection limited, leading to additional surface charge σ accumulating at the interface between the organic semiconductor layers and the injecting contact.[23] The most efficient OLED's employ a heterostructure[24] to force exciton formation and luminescence to occur far from the electrodes. This typically prevents charge from leaking through the device without first forming excitons, and provides spatial confinement of the excited states. In a conventional OLED such as that of Fig. 1(b), the surface charge at the injection contact is balanced by positive charge at the interface of the hole and electron transport layers (HTL and ETL). The injection-limited charge is related to the applied voltage V by

$$n = \frac{\varepsilon V}{q d_I d_{\mathrm{ETL}}}, \tag{4}$$

where d_{ETL} is the thickness of the electron transport layer and the HTL/ETL interfacial charge is given by $\sigma = n d_I$, where d_I is the thickness of the exciton formation zone [see Fig. 1(b)].

Triplets are formed by the direct combination of electrons and holes, as well as via intersystem crossing from the singlet state. In fluorescent materials, triplets rarely luminesce, and the dominant decay paths are via nonradiative coupling to a vibronic excitation of the molecular ground state, triplet-triplet annihilation, and triplet-polaron quenching. Typically, triplets do not participate in long-range Förster energy

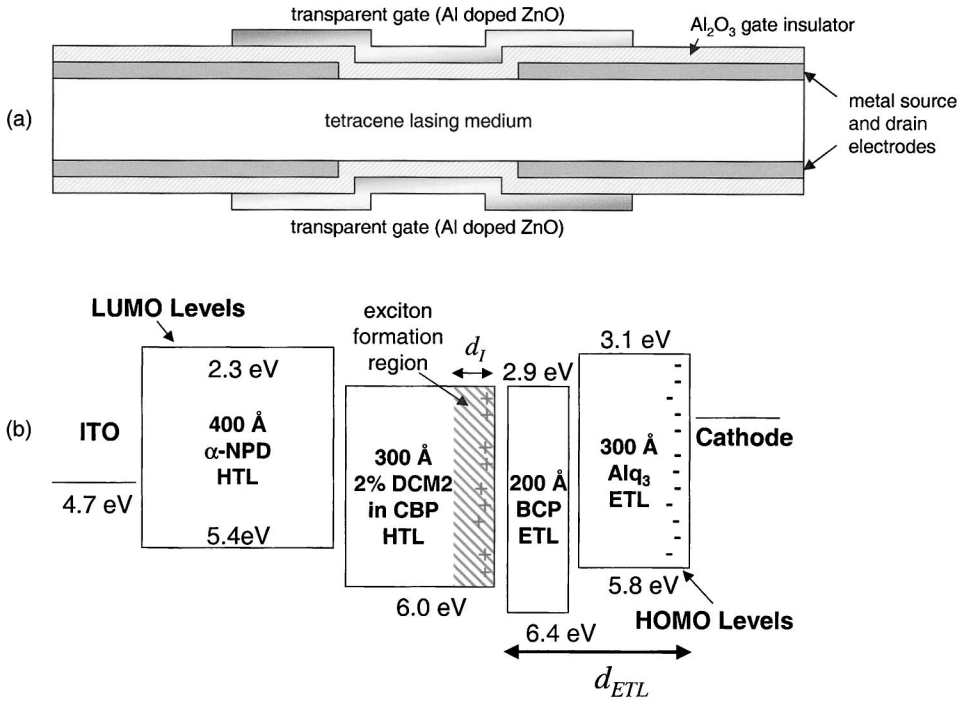

FIG. 1. (a) The structure of the tetracene device of Schön *et al.* (Ref. 1). Two thin-film transistors are fabricated on either side of a single crystal of tetracene. The source and drain electrodes are formed by thermal evaporation through a shadow mask of gold (for hole injection) and aluminum (for electron injection). The gate insulator is a sputtered film of amorphous aluminum oxide and the gate electrodes are transparent aluminum doped zinc oxide. By applying high voltages to the gate electrodes, charge is efficiently injected into the crystal interfaces. Electroluminescence occurs when a slight bias is placed across the crystal. A Fabry-Perot cavity is formed perpendicular to this cross section by cleaving the crystal. The length of the thin-film transistors in Ref. 1 is 25 μm and the cavity length is $\approx$750 μm. The thickness of the crystal is $\approx$10 μm (b). The architecture and energy levels of a typical high-efficiency amorphous OLED. The device is injection limited and a large amount of negative charge is located at the cathode. A corresponding amount of positive charge is retained in the exciton formation region, adjacent to the BCP hole-blocking layer. The positive charge quenches excitons, reducing the quantum efficiency. Preferentially electron and hole transporting layers are represented by ETL and HTL, respectively. We also indicate the thickness *d* of the organic layers separating the cathode from the hole-blocking interface. Note that we have assumed that the HOMO-LUMO gap is equal to the optical energy gap, as determined from absorption spectra. Under this assumption, the LUMO does not necessarily serve as the lowest conduction level for mobile electrons. Although not shown here, charge redistributions and polarization effects at the heterointerfaces are expected to alter the relative energy-level alignments when differing materials are brought into contact (Ref. 57).

transfer,[25] so triplet-polaron quenching requires a collision between the species, and hence is much slower than singlet-polaron quenching.

Triplet-triplet annihilation is characterized by rate κ'_{TT} as follows:

$$T^*+T^* \xrightarrow{\kappa'_{\mathrm{TT}}} T^*+S, \qquad T^*+T^* \xrightarrow{\xi\kappa'_{\mathrm{TT}}} S^*+S, \tag{5}$$

where T^* represents the excited triplet exciton. When two triplets collide, spin statistics[26] determine the probability of singlet and triplet formation. It is often assumed that the generation rate of singlets from uncorrelated charges is $\frac{1}{3}$ times that of triplets,[17] i.e., $\xi=\frac{1}{3}$ and $8T^*\rightarrow 3T^*+S^*+4S$.

Triplet-polaron (T^*-P) quenching occurs as follows:

$$T^*+P \xrightarrow{\kappa_{\mathrm{TP}}} S+P. \tag{6}$$

A typical rate, κ_{TP}, for triplet-polaron quenching in amorphous films is 1×10^{-12} cm^3/s.[23,27] Intersystem crossing is simply

$$S^* \xrightarrow{k_{\mathrm{ISC}}} T^*, \tag{7}$$

governed by the rate k_{ISC}.

Including all of these processes, the rate equation for the triplet exciton concentration N_T is

$$\frac{dN_T}{dt}=-k_{\mathrm{NR}}^T N_T-\kappa_{\mathrm{TP}} n N_T-\kappa_{\mathrm{TT}} N_T^2+K_{\mathrm{ISC}} N_S+\frac{1}{1+\xi}\frac{J}{qd_I}, \tag{8}$$

where k_{NR}^T is the rate of nonradiative triplet decay, N_S is the singlet density, q is the electronic charge, and the total loss rate of triplets is given by $\kappa_{\mathrm{TT}}=(\frac{1}{2}+\xi)\kappa_{\mathrm{TT}}'$.

Assuming that the rate of triplet generation from intersystem crossing is much less than the rate of electrical generation of triplets, i.e., (k_{ISC} small), the transient solution to Eq. (8) is

$$N_T(t)=\left(\frac{3J}{2qd_I(k_{\rm NR}^T+\kappa_{\rm TP}n)}\right)\times\frac{1-\exp[-\Delta(k_{\rm NR}^T+\kappa_{\rm TP}n)t]}{(1+\Delta)-(1-\Delta)\exp[-\Delta(k_{\rm NR}^T+\kappa_{\rm TP}n)t]}, \quad (9)$$

where $\Delta=\sqrt{1+3J\kappa_{\rm TT}/qd_I(k_{\rm NR}^T+\kappa_{\rm TP}n)^2}$ and $N_T=0$ at time $t=0$. At the low injection levels often used in OLED's (i.e., $J\sim 1$ mA/cm^2), $\Delta\sim 1$ and Eq. (9) may be approximated by

$$N_T=\frac{3J}{4qd_Ik_{\rm NR}^T}(1-\exp[-k_{\rm NR}^Tt]). \quad (10)$$

For electrically pumped lasing, much higher injection levels are expected, and we may assume that triplet losses from triplet-triplet and triplet-polaron annihilation are dominant. In this case, the steady-state solution of Eq. (8) using Eq. (3) is

$$N_T=\frac{\kappa_{\rm TP}}{2\kappa_{\rm TT}}\left(-1+\sqrt{1+\frac{6\kappa_{\rm TT}\mu dq}{\kappa_{\rm TP}^2\varepsilon d_I}}\right)\sqrt{\frac{\varepsilon J}{2\mu dq^2}}. \quad (11)$$

The loss mechanisms for singlet excitons are singlet-triplet annihilation at rate κ_{ST},

$$T^*+S^*\xrightarrow{\kappa_{\rm ST}}T^*+S, \quad (12)$$

singlet-singlet annihilation [see Eq. (2)], and singlet-polaron annihilation at rate $\kappa_{\rm SP}$,

$$S^*+P\xrightarrow{\kappa_{\rm SP}}S+P. \quad (13)$$

The rate equation for singlet excitons is, therefore,

$$\frac{dN_S}{dt}=-k_RN_S-k_{\rm NR}^SN_S-k_{\rm ISC}N_S-\kappa_{ST}N_SN_T-\kappa_{\rm SP}nN_S-\tfrac{1}{2}\kappa_{\rm SS}N_S^2+\frac{\xi}{1+2\xi}\kappa_{\rm TT}N_T^2+\frac{\xi}{1+\xi}\frac{J}{qd_I}, \quad (14)$$

where k_R is the radiative rate of singlet fluorescence and $k_{\rm NR}^S$ is the intrinsic nonradiative rate of singlets. The coupled pair of Eqs. (8) and (14) can be solved in steady state to give the singlet density as a function of J. At very high singlet densities, Eq. (14) is dominated by singlet-singlet annihilation. Equations (3) and (11) demonstrate that triplets and polarons should increase with $\sqrt{J}$ in electrically pumped lasers, and Eq. (14) indicates that singlet losses from singlet-singlet annihilation also increase with $\sqrt{J}$. Under these conditions, the steady-state quantum efficiency may be expressed as[27]

$$\frac{\eta}{\eta_0}=\frac{J_0}{4J}\left(\sqrt{1+8\frac{J}{J_0}}-1\right). \quad (15)$$

where η_0 is the quantum efficiency in the absence of singlet-singlet annihilation, and

$$J_0=\frac{4qd_I}{\kappa_{\rm SS}\tau^2} \quad (16)$$

is the annihilation ''onset'' current density at $\eta=\eta_0/2$.

B. Electric-field and power dependent nonradiative losses

When a potential is applied across an amorphous organic film, the resulting hole and electron currents typically vary substantially in magnitude, reducing the quantum efficiency of a single-layer OLED. Unbalanced hole and electron currents may arise from differences in injection efficiency or charge transport mobility. But by use of a heterostructure, it is possible to force balanced current flow by introducing barriers to the leakage of charge carriers out of the luminescent region.[24] A heterostructure may be fabricated from a material that predominantly transports electrons, together with a material that predominantly transports holes. Or, a large energy barrier at the heterointerface may retard the flow of either electrons or holes. In this section, we examine efficiency losses that result from the breakdown of charge confinement in a heterostructure at high electric fields. Electric-field-induced losses from exciton dissociation have been studied previously in OLED materials.[28] However, in a heterostructure device, charge confinement should force any dissociated charges to eventually re-form an exciton. In any case, the binding energy of most excitons in amorphous films of small molecular weight materials is $\sim$1 eV (for example, the binding energy of an Alq_3 singlet is 1.4 eV).[29] Thus, maintenance of charge confinement is fundamental to the efficient operation of an OLED.

First, we examine the effect of high fields in structures that confine charges with a mobility gap. We consider a luminescent layer in a heterostructure OLED that preferentially transports majority carriers with density n_M and mobility μ_M. Preferential hole or electron transport is a property of materials with widely varying charge transport mobilities, i.e., a predominantly electron transporting material has $\mu_e \gg \mu_h$, where μ_e and μ_h are the electron and hole mobilities, respectively. The heterostructure confines the majority carriers but allows the injection of minority carriers with density n_m and mobility μ_m. An example is the archetypical[24] Alq_3/N,N'-diphenyl-N,N'-bis(3-methylphenyl)-(1,1'-biphenyl)-4,4'-diamine (TPD) heterostructure OLED. TPD preferentially transports holes, and its small electron mobility forces exciton formation to occur in Alq_3. Electrons are preferentially transported in Alq_3, but holes can be injected from TPD, although they are in turn confined by the relatively small hole mobility of Alq_3.

To calculate losses within the heterostructure shown schematically in Fig. 2, we describe the dynamics of the minority carriers using

$$\frac{dn_m}{dt}=-\kappa_Ln_Mn_m-\frac{\mu_mF}{d_L}n_m+\frac{J}{qd_L}, \quad (17)$$

where the rate of electron-hole combination is commonly described by Langevin theory,[17,30] viz., $\kappa_L=q(\mu_M+\mu_m)/\varepsilon$, and F is the electric field. The luminescent layer (thickness, d_L) extends from the heterostructure interface to the injecting contact. We assume that because of energy transfer to surface polaritons and other nonradiative losses,[31] all luminescence is quenched in a region of thickness Δx

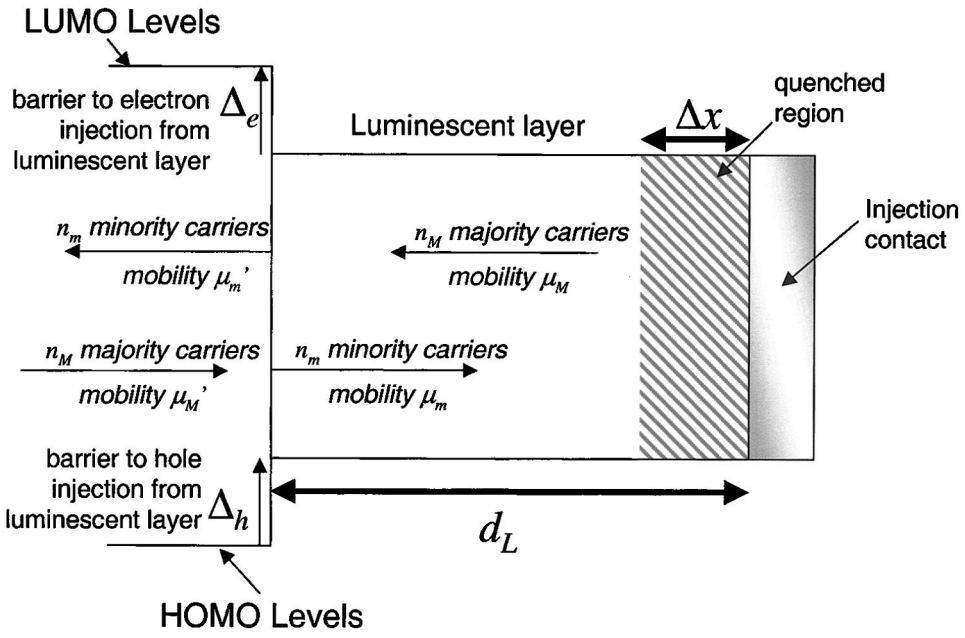

FIG. 2. A schematic heterostructure with parameters shown for the determination of field-induced exciton losses. Majority carriers are confined within the luminescent layer by a combination of energy barriers (Δ_e and Δ_h) and mobility steps ($\mu_M \gg \mu_m'$). Minority carriers are injected from the organic transport material, where they combine with majority carriers to form excitons. Close to the injecting contact, however, the excitons are quenched by energy transfer. The fraction of charges that form excitons outside this region is defined as the efficiency of charge confinement, η_C; see Eq. (20) in text.

adjacent to the injecting contact. The second term in Eq. (17) is the residence time of a minority carrier, and the last term accounts for the flow of minority carriers into the luminescent layer under bias.

We find in Sec. IV A that current flow is space-charge limited at the very high injection levels required in organic lasers. Thus, under this model,

$$\frac{dn_m}{dx} = \frac{q(\mu_m + \mu_M) n_M}{\varepsilon \mu_m F} n_m, \tag{18}$$

where x is the distance from the injecting contact. Assuming that the electric field close to the injecting contact is determined by the majority carriers, i.e.,

$$F = 2qn_M x/\varepsilon, \tag{19}$$

the solution to Eq. (18) is

$$\eta_C = 1 - [n_m(\Delta x)/n_m(d_L)] = 1 - [\Delta x/d_L]^{(\mu_m + \mu_M)/2\mu_m}, \tag{20}$$

where η_C is the efficiency of charge confinement in the heterostructure, defined as the fraction of injected charges that form excitons. Since $\mu_M \gg \mu_m$, $\eta_C \sim 1$ in most heterostructure OLED's. At high electric fields, $\mu_m \rightarrow \mu_M$, then $\eta_C \rightarrow (1 - \Delta x/d_L)$. The thickness of the nonradiative region adjacent to the cathode is $\Delta x \sim 100$ Å, thus for a typical luminescent layer of thickness $d_L \sim 600$ Å, the minimum possible charge confinement efficiency is $\eta_C = 80\%$. This suggests that single-layer OLED's are potentially very efficient if both carriers can be injected into organic layers with similar efficiencies.

Energy barriers may also be used to confine charge carriers. However, since the interfacial energy barrier is typically $\Delta \sim 1$ eV, the electric field required to break charge confinement is $F = \Delta/\delta \sim 10^7$ V/cm, where we have taken the width of the interface, $\delta = 10$ Å. This is similar to that required for dielectric breakdown and catastrophic failure of the device. Thus, field-induced nonradiative losses are not likely to dominate in a well-designed organic heterostructure.

III. THEORY OF NONRADIATIVE LOSSES AND LASING

We now determine the impact of the nonradiative losses considered in Sec. II on the threshold of an electrically pumped organic laser. The internal quantum efficiency of fluorescence in the laser cavity is

$$\eta_{\mathrm{INT}} = \frac{k_R N_S}{J/qd_I} = \frac{k_R}{k_R + k_{\mathrm{NR}}(T,J)}, \tag{21}$$

where $k_{\mathrm{NR}}(T,J)$ is the aggregate rate of nonradiative singlet decay dependent on temperature T and current density. Typically, only a fraction χ of the fluorescence is emitted externally, i.e., $\eta_{\mathrm{EXT}} = \chi \eta_{\mathrm{INT}}$. For example, in surface emitting OLED's fabricated on flat glass substrates, only ~20% of photons are emitted in the forward or viewing direction.[13] The remainder is lost to waveguiding in the substrate, or by nonradiative coupling to surface plasmons at the metal/organic contact interfaces.[31,32]

Now, the population density of singlets at the threshold of lasing is[33]

$$N_S^{\mathrm{TH}} = \frac{8\pi n_r^2}{\Gamma g(\lambda) \lambda^2 k_R} \left(\alpha_0 - \frac{1}{L} \ln(R) \right) = \frac{8\pi n_r^2}{\Gamma g(\lambda) \lambda^2 k_R} \alpha_T, \tag{22}$$

where $g(\lambda)$ is the normalized fluorescent spectrum of the laser dye, n_r is the cavity refractive index, α_0 is the optical absorption coefficient of the cavity at the lasing wavelength λ_0, L is the length of the cavity, R is the reflectivity of each mirror (both assumed equal for simplicity), Γ is the optical confinement factor within the active layer, and α_T is the total cavity absorption coefficient. In organic electroluminescent devices, the thickness of the exciton formation zone, $d_I \sim 100$ Å, is expected to be much less than the diameter of

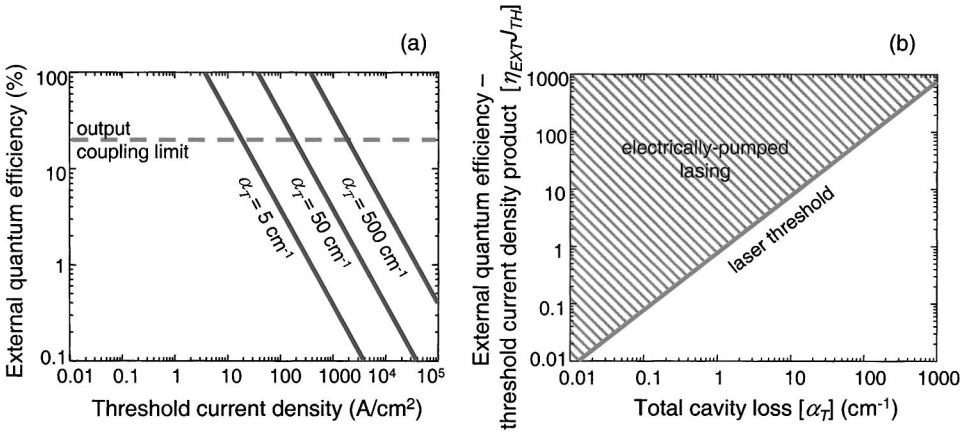

FIG. 3. To test the potential of an electroluminescent film for use in an electrically pumped laser, it can be incorporated in an OLED. Then, by measuring the external quantum efficiency of an OLED, these charts allow the material and device architecture to be evaluated. In (a), the quantum efficiency-current–density thresholds are shown as a function of current density for several values of the total cavity loss, which comprises mirror losses, optical absorption, and polaron absorption. In (b), we show the minimum quantum efficiency-current density as a function of total cavity loss.

the optical mode.[30] Hence, we can approximate the optical confinement factor as $\Gamma = A_0 d_I$, allowing for the elimination of d_I from the expression for the threshold current density [see Eq. (24) below]. To a first approximation, therefore, the confinement factor is independent of the charge transport properties of the organic materials. Improvements in Γ may be achieved by increasing the refractive index of the laser waveguide. Combining Eqs. (21) and (22) then gives

$$\gamma = \frac{\eta_{\mathrm{INT}} J}{q d_l} \frac{\Gamma \lambda^4}{8\pi n_r^2 c \Delta\lambda}, \tag{23}$$

$$\eta_{\mathrm{EXT}} J_{\mathrm{TH}} > \chi \frac{8\pi n_r^2 q c \Delta\lambda}{A_0 \lambda^4} \left(\alpha_0 - \frac{1}{L} \ln(R) \right). \tag{24}$$

where γ is the maximum optical gain (i.e., in the absence of absorption and mirror losses) and J_{TH} is the threshold current density. We have approximated the normalized spectrum at the lasing frequency by $g(\lambda_0) \approx {\lambda_0}^2 / c\Delta\lambda$. Here $\Delta\lambda$ is the spectral width of the laser dye.[33]

Values of the laser operating parameters for a molecular solid are typified by the dye DCM2,[34] with $\lambda_0 \sim 650$ nm, $\Delta\lambda \sim 70$ nm, and $k_R \sim 2\times 10^8$ s^{-1}. Thus, from Eq. (22) electrically pumped lasing typically requires $N_S^{\mathrm{TH}} > 4 \times 10^{15} (\alpha_T/\Gamma)$ cm^{-3}. Kozlov *et al.*[11] have measured $\alpha_0 = (27 \pm 4)$ cm^{-1} in an electrically pumped structure consisting of 200-Å-thick ITO cathodes and anodes, enclosing organic layers with a total thickness of 1000 Å. For a cavity length of $L = 1$ mm, and using the organic/air interface as a reflecting surface (giving $R \sim 7\%$), a mirror loss of $-(1/L)\ln(R) = 27$ cm^{-1} is obtained, resulting in a total loss of $\alpha_T = (54 \pm 4)$ cm^{-1}. This does not include nonradiative losses; these are included in the quantum efficiency η in Eqs. (23) and (24). For a typical laser structure with a 1000-Å-thick organic layer of refractive index $n_r = 1.72$ and a 2% DCM2:Alq_3 active region of refractive index $n_r = 1.78$, the confinement factor within the organic structure is[11] $\Gamma = 40\%$, giving $A_0 = 4 \times 10^4$ cm^{-1}. Furthermore, for typical surface emitting OLED's, the output coupling fraction χ is ≈ 0.2.[13] The minimum external quantum efficiency-threshold-current–density product is then $\eta_{\mathrm{EXT}} J_{\mathrm{TH}} > 40$ A/cm^2, allowing us to define the performance required of an electroluminescent material if it is to be considered for use in an electrically pumped laser; i.e., for a typical external fluorescent quantum efficiency of $\eta_{\mathrm{EXT}} = 2\%$, the required threshold current density for a Fabry-Perot laser is $J_{\mathrm{TH}} = 2$ kA/cm^2. To our knowledge, this value of J_{TH} is somewhat higher than has been obtained in the amorphous organic electroluminescent devices studied to date,[11,15] although it is achievable in high-mobility crystalline materials such as tetracene.[1]

Figure 3 summarizes the analysis of the quantum efficiency-threshold current density product: the upper bound to efficiency is the output coupling fraction $\chi \sim 0.2$, since an external efficiency of $\eta_{\mathrm{EXT}} \sim 20\%$ corresponds to a device with 100% internal quantum efficiency.[13] We must also consider the additional polaron absorption induced by electrical excitation, although we note that lasing materials that possess efficiencies that are relatively independent of current density are also not likely to exhibit significant polaron absorption, since the process of singlet-polaron annihilation is closely related. At a current density of $J = 100$ A/cm^2, Kozlov *et al.*[11] found that the absorption of a DCM2:Alq_3 device increased to $\alpha_T = 400$ cm^{-1}, increasing the threshold to $\eta_{\mathrm{EXT}} J_{\mathrm{TH}} = 300$ A/cm^2. It is shown in Sec. IV A that DCM2 also exhibits strong singlet-polaron annihilation, in agreement with the expected link with polaron absorption.

Alternately, it is possible to design a distributed feedback laser where the mirror loss is nearly zero;[11] and for a material system without polaron absorption, it is conceivable that the cavity loss may be as low as $\alpha_T \sim 5$ cm^{-1}. Indeed, in an optically pumped laser, cavity losses as low as $\alpha_T \sim 1$ cm^{-1} have been demonstrated.[11] Thus, in Fig. 3(a) we show J_{TH} for several values of cavity loss between $\alpha_T = 5$ and 500 cm^{-1}. In Fig. 3(b), the minimum quantum efficiency-

threshold current density product is plotted as a function of cavity loss. Under the most favorable conditions of low loss, high optical confinement, and high quantum efficiency, $\eta_{EXT} \rightarrow 5\%$, threshold currents as low as 50 A/cm^2 may be sufficient for electrically pumped lasing in small-molecule polymeric and crystalline films.

IV. ANALYSIS OF AMORPHOUS AND CRYSTALLINE LASER STRUCTURES

A. Measurements of nonradiative losses in amorphous films

To understand the effects of nonradiative losses in electrically pumped amorphous thin films, we studied an archetype guest-host system consisting of 2% DCM2 in 4,4′-*N*,*N*′-dicarbazole-biphenyl (CBP). As discussed above, the rate of singlet-polaron quenching is determined by the overlap between the singlet fluorescence and polaron absorption spectra. In a film of DCM2:CBP, there is overlap between CBP fluorescence and DCM2 absorption, and the Förster radius for singlet transfer is $R \sim 30$ Å.[35] Consequently, there is likely to be strong absorption and quenching of CBP singlets by DCM2 polarons, which may preferentially accumulate on DCM2 rather than CBP because of the narrower energy gap of DCM2.

Electrical pumping of DCM2:CBP is achieved by incorporating it as the emissive layer of an OLED, and in Fig. 1(b) we show the proposed energy-level diagram for the device. The electron energy levels are indicated by the lowest unoccupied molecular orbitals (LUMO's) and those of holes are given by the highest occupied molecular orbitals (HOMO's). The HOMO is determined from the ionization potential for each material referenced to vacuum,[36] and the LUMO position is approximated by the difference of the ionization potential and the optical energy gap.

Organic layers were deposited by high-vacuum (10^{-6} Torr) thermal evaporation onto a cleaned glass substrate precoated with transparent, conductive ITO. A 400-Å-thick layer of 4,4′-bis[*N*-(1-napthyl)-*N*-phenyl-amino] biphenyl was used to transport holes to the luminescent layer consisting of either CBP or 2% DCM2 in CBP. A 300-Å-thick layer of Alq_3 was used to transport electrons into the emissive layer and to reduce DCM2 luminescence absorption at the cathode. We use a thin (200-Å) barrier layer of 2,9-dimethyl-4,7-diphenyl-1,10-phenanthroline (bathocuproine or BCP) to confine holes and excitons within the luminescent DCM2:CBP layer.[37]

From an analysis of the behavior of Alq_3/metal contacts, it has been determined that transport in Alq_3 is injection limited by electron trapping at the Alq_3/metal interface.[23] To maintain charge neutrality, the corresponding positive charge is constrained by the hole-blocking layer of BCP at the CBP/BCP interface. Thus, the OLED structure of Fig. 1(b) maximizes singlet-polaron quenching within the luminescent layer. For simplicity, we neglect both the potential required to inject and transport holes, and the built-in potential of this device, and assume that the distance d_{ETL} separating the two charged layers determines the total voltage across the device.

The density of the interfacial charge is adjusted by varying the injection properties of the cathode.[23] Hence, we fabricated OLED's using three different cathode materials: LiF/Al, Mg:Ag, and Al. The LiF/Al cathode possesses the most efficient electron-injecting characteristics, consisting of a 5-Å-thick layer of LiF capped with a 1000-Å-thick layer of Al deposited through a shadow mask with 1-mm-diameter openings. Magnesium-silver cathodes are the next most efficient electron injectors; they consisted of a 1000-Å-thick layer of 25:1 Mg:Ag, with a 500-Å-thick Ag cap. We also used cathodes consisting of only a single 1000-Å-thick layer of Al. These required the largest voltage to achieve a given current density, and consequently they maximize the density of charge at the CBP/BCP interface. Due to injection-limited transport and the large density of charge in the emissive layer, we expect singlet-polaron quenching to be much greater than singlet-triplet quenching and singlet-singlet annihilation. Thus, we can neglect the N_s^2 and triplet terms in Eq. (14), and fit the quantum efficiency to

$$\eta_{EXT} = \frac{\eta_0}{1 + \kappa_{SP}\tau\varepsilon / q d_I (V/d_{ETL})}, \tag{25}$$

where τ is the exciton lifetime ($\tau^{-1} = k_R + k_{NR}^s + k_{ISC}$) and the unquenched quantum efficiency is $\eta_0 = \chi k_R / (k_R + k_{NR}^s + k_{ISC})$. As $V_{ETL} \rightarrow 0$, the quantum efficiency (i.e., η_0) may not be meaningful, rather it should be used as a scaling parameter.

In Fig. 4, the quantum efficiencies of DCM2:CBP fluorescent devices employing different cathodes are plotted versus current and voltage. To confirm the expected dependence of quenching on the thickness d_{ETL}, an additional device was made with 600 Å of Alq_3 instead of the 300 Å shown in Fig. 1. With the addition of the 200-Å-thick BCP hole-blocking layer, this device has $d_{ETL} = 800$ Å. Since the emission zone in this case is 300 Å further from the metal cathode, the OLED quantum efficiency was reduced by 20% due to the influence of the optical microcavity.[32]

When the quantum efficiency of these devices is plotted against J in Fig. 4(a) we find no consistency between the performance of the various devices. But when quantum efficiency is plotted against voltage in Fig. 4(b), there is good agreement with Eq. (25), as indicated by the solid line. Since the quenching rate is expected to be proportional to V/d_{ETL}, in Fig. 4(b) we adjust the abscissa for the thicker device ($d_{ETL} = 800$ Å) so that it can be compared to the three devices with $d_{ETL} = 500$ Å. Indeed, this enables us to fit the data from all four devices to obtain $\kappa_{SP}\tau\varepsilon / q d_{ETL} d_I = 0.42\ \mathrm{V}^{-1}$, corresponding to a singlet-polaron quenching rate of $\approx \kappa_{SP} = 3 \times 10^{-10}$ cm^3/s. From Eq. (1), and assuming a Förster radius for singlet-polaron quenching of $R \sim 30$ Å,[35] we obtain a singlet diffusion constant of $D \sim 1 \times 10^{-4}$ cm^2/s, about two orders of magnitude lower than the singlet diffusion coefficient in a crystalline material such as tetracene.[17] Thus, the rate of singlet quenching in amorphous materials should be less than that in crystalline materials by a similar factor. Since the optical transitions of singlet excitons conserve spin, Förster energy transfer of singlets is typically faster than triplet energy transfer, so we expect singlet-polaron quenching to be larger than triplet-polaron quenching. Transient studies of electrophosphorescent de-

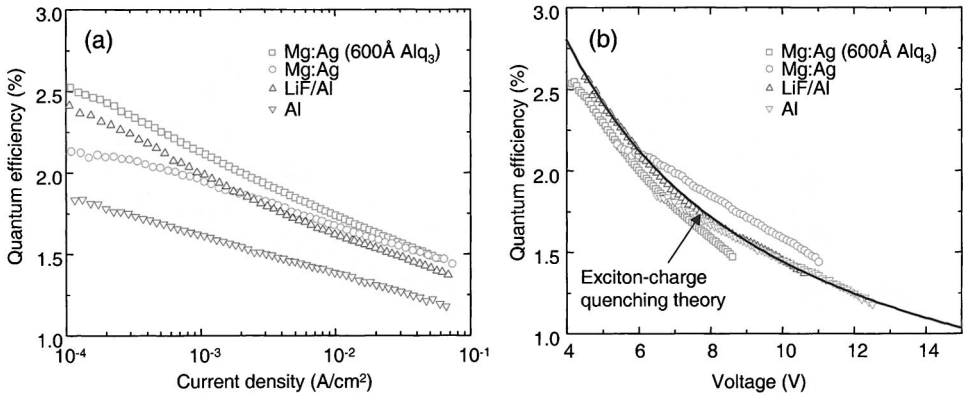

FIG. 4. (a) The characteristics of four fluorescent devices with general structure given by Fig. 1(b). For the three devices with varying electron-injection contacts, the quantum efficiency at a given current density also varies. In (b), however, it is found that the quantum efficiencies of these three devices at a given voltage are approximately identical. The fourth device has a thicker Alq_3 layer, in order to test the thickness dependence of Eq. (25). Thus, for comparison, the quantum efficiency of this device has been plotted against the same electric field ($F=V/d$) as the other three devices. Good agreement is found between the behavior of these four devices and the exciton-polaron quenching theory (solid line) of Eq. (25), where $\eta_0=7.5\%$ and $k_{SP}\tau\varepsilon/qd_{ETL}d_1=0.42\ V^{-1}$.

vices have yielded $\kappa_{TP}=1\times10^{-12}$ cm^3/s.[23] Because current transport in the device is limited by electron injection, the field in the HTL is $<10^5$ V/cm, and is not expected to cause significant dissociation of DCM2 excitons (cf. Sec. II B).

Finally, we examine the current-voltage characteristics of the OLED at high injection levels. The structure used differs from that of Fig. 1(b) by the omission of DCM2 from the CBP layer. To prevent damage due to device heating,[38,39] pulses of between 700 ns and 70 μs duration at a duty cycle of $<0.02\%$ are applied at current densities above $J\sim1$ A/cm^2. The expected temperature increase is calculated using values for the heat capacity, thermal conductivity, and density of the 1-mm-thick glass substrate of 710 J/kg K, 1.32 W/K m, and 2200 kg/m^3, respectively.[40] For a maximum applied bias of 40 V and $J=40$ A/cm^2, we calculate that the device temperature increases with time t as $\Delta T[1-\exp(-t/\tau)]$, with a characteristic time $\tau=1$ s, and where ΔT is the temperature increase in steady state. For 70-μs pulses, we expect an insignificant temperature increase. Charge transport and injection are sensitive to temperature,[23,41] and the absence of heating is confirmed by the current-voltage characteristics of the OLED's, which show no change as the pulse width is reduced to 700 ns.

Injection-limited transport in OLED's is characterized by a current density that increases superlinearly with voltage (i.e., $J\sim V^m$, $m\cong8$).[23] But the pulsed current-voltage characteristic shown in Fig. 5 demonstrates that the power-law slope m is reduced at the highest current densities as the interfacial states are filled, and transport approaches the bulk space-charge limit[11,15] (dotted line, Fig. 5). Thus, at the high-

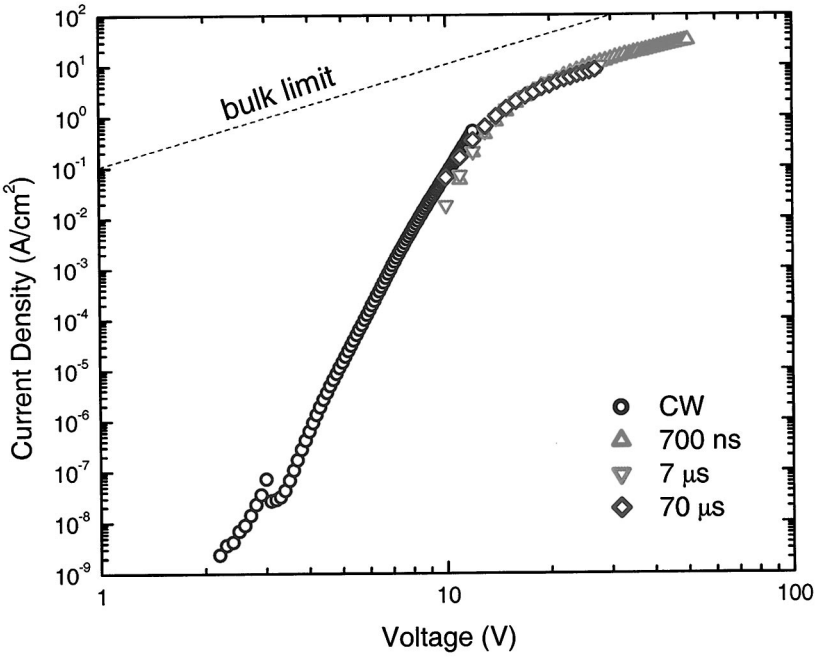

FIG. 5. The current-voltage characteristics of the OLED shown in Fig. 1(b), with a neat film of CBP rather than the emissive layer of DCM2:CBP. At high current densities, pulsed bias was applied. The change in power-law slope is indicative of a transition from injection-limited to bulk-limited transport. The bulk limit is shown by the dotted line, calculated for an Alq_3 charge-carrier mobility of $\sim10^{-4}$ cm^2/V s (Ref. 58).

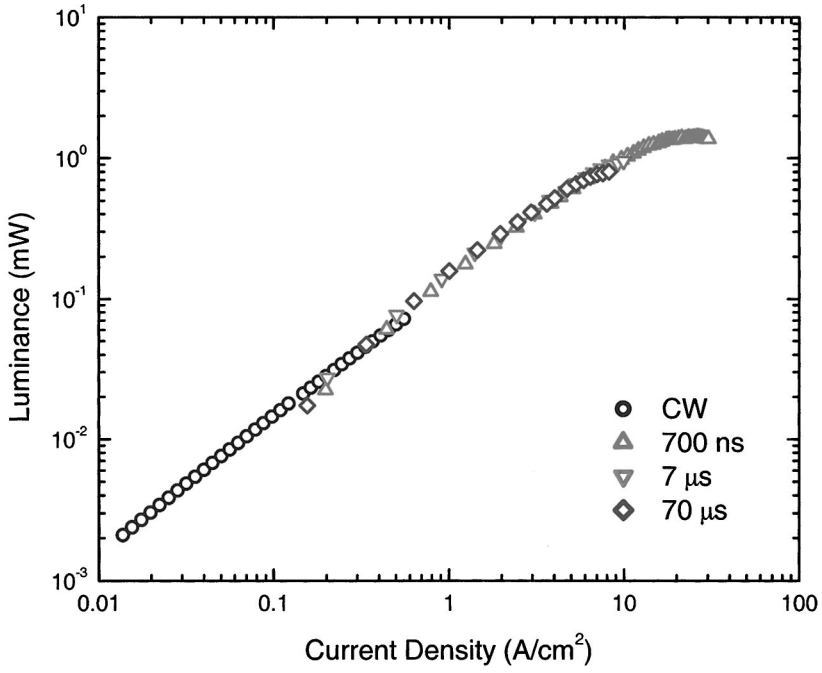

FIG. 6. The emissive optical power of the CBP/BCP OLED's is linear with respect to the applied current density for $J<3$ A/cm^2. The power eventually saturates, demonstrating that losses increase significantly at high excitation strength.

est current densities required for lasing, the polaron density is ultimately determined by the bulk transport properties (e.g., the mobility) of the emissive organic film [see Eq. (3)].

If the DCM2 is removed from the device shown in Fig. 1(b), fluorescence is observed from the BCP/CBP interface. Singlet-polaron losses are reduced due to the weak overlap between fluorescence and the absorption of CBP and BCP polarons. In Fig. 6 we show the luminescent output power of the OLED as a function of current density. For this measurement, light was collected by a silicon detector.[42] The pulsed measurements of luminescence are consistent with CW measurements at low intensity. The response is linear up to $J \sim 3$ A/cm^2, in contrast to the data of Fig. 4(b). However, at higher injection levels, the devices begin to degrade, most probably due to the destruction of the BCP layer, a failure mechanism that also occurs slowly at much lower current densities.[43] At $\approx J=40$ A/cm^2, the cathodes fail catastrophically via a separate mechanism, ultimately limiting the maximum external quantum efficiency-current–density product to $\eta_{EXT}J=0.06$ A/cm^2 (see Fig. 7). This is approximately two orders of magnitude below that required for lasing in an optimized structure.

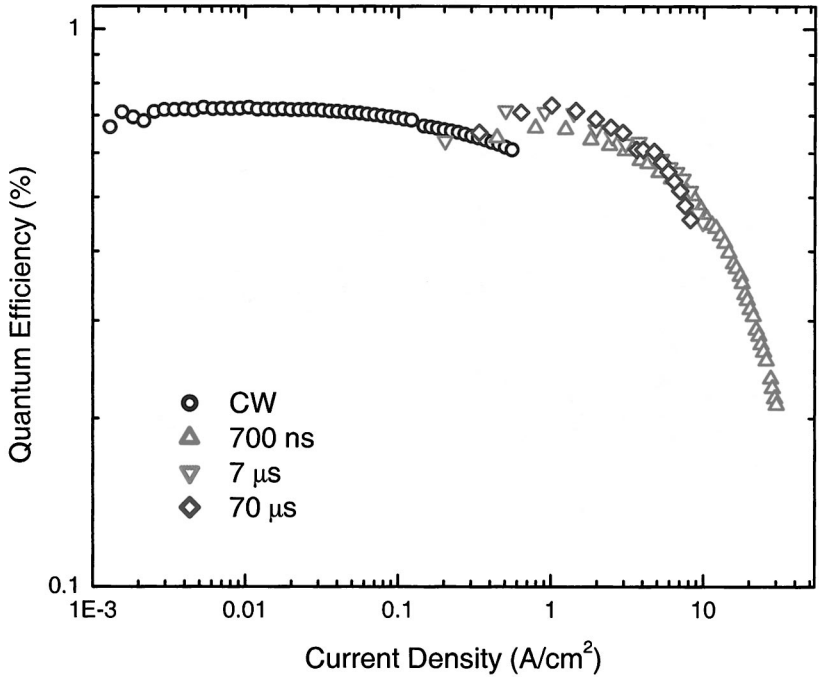

FIG. 7. The quantum efficiency of CBP/BCP OLED's as a function of applied current density for three different excitation conditions: steady state, 70-μs pulses, 7-μs and 700-ns pulses. The devices fail at $J=40$ A/cm^2. The peak external quantum efficiency-current–density product is $\eta_{EXT}J=0.06$.

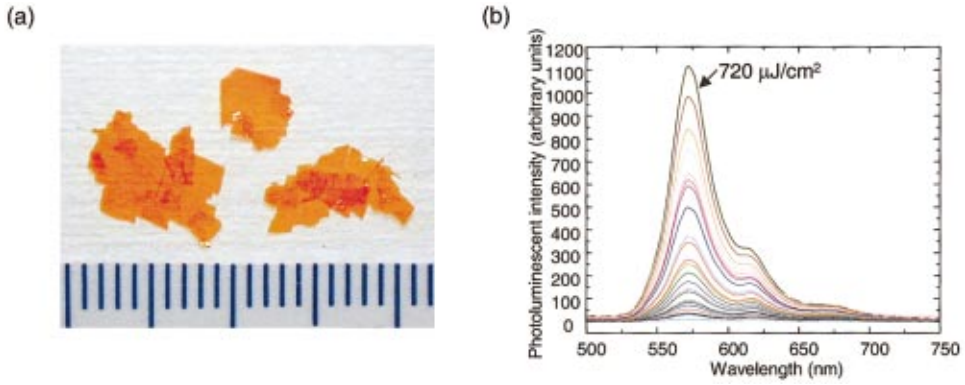

FIG. 8. (Color) (a) A photograph showing a typical tetracene crystal used in the measurement of quantum yield in (b). The crystal is ≈10 mm long and 10 μm thick. The crystals surfaces are terraced, with smooth areas of up to ~1 mm^2. For optical pumping experiments, the crystals were cut to form parallel facets. (b) The photoluminescent spectra of tetracene under increasing intensities. No significant narrowing is observed for $N_S < 10^{16}$ cm^{-3}.

B. The crystalline tetracene of Schön *et al.*

To our knowledge, the crystalline organic material tetracene is the first organic material to show gain under electrical pumping.[1] In Sec. IV B 1 we examine the published characteristics of the structure used to demonstrate gain. The nonradiative losses in crystalline tetracene are examined in Sec. IV B 2, and the optics and relevant physics in the bulk and at interfaces are discussed in Secs. IV B 3 and IV B 4, respectively.

1. Characteristics of the tetracene device

The structure given by Schön *et al.*[1] is shown in Fig. 1(a). Charge is injected using dual thin-film transistors that allow both hole and electron currents to be individually tuned. When a small potential is placed across the device, hole and electron currents are injected into the bulk, forming excitons. A Fabry-Perot cavity is formed perpendicular to the cross section of Fig. 1(a) by cleaving the crystal. The gate length of the thin-film transistors in Ref. 1 is 25 μm and the cavity length is ≈750μm. The thickness of the crystal is ≈2–10 μm.[44]

The five unambiguous characteristics of lasing according to Kozlov *et al.*[3] are (1) a clear indication of a threshold in output energy as a function of input energy, with a high lasing efficiency above threshold, (2) strong output beam polarization in confined cavities, (3) spatial coherence (as indicated by a diffraction-limited output beam or speckle), (4) significant spectral line narrowing, and (5) the existence of laser cavity resonances, or modes. The device of Schön *et al.*[1] shows strong evidence for optical gain, as demonstrated by significant spectral line narrowing ($\Delta\lambda \sim 2.5$ Å at $J = 2000$ A/cm^2 and $T = 5$ K). There is also evidence of Fabry-Perot resonances in the tetracene spectrum, although such weak resonances are frequently observed below threshold in conventional semiconductor lasers.[45] However, the threshold in Ref. 1 is not well defined, no evidence of a beam is presented, the spectral line continues to decrease above threshold uncharacteristic of lasing, and the slope efficiency is only $\sim 10^{-4}$, apparently confirming that the device is operating below threshold at both $T = 5$ and 300 K. The poor slope efficiency indicates that an extremely small fraction of the injected charge is contributing to electroluminescence emerging from the facets. These observations suggest that the device of Ref. 1 is possibly a superluminescent OLED.[45]

In the remainder of this section, the operation of the tetracene device is analyzed in detail. First, we consider nonradiative losses in Sec. IV B 2 and find that singlet-singlet annihilation leads to significant reductions in efficiency at high injection levels. Tetracene also has a relatively poor photoluminescent efficiency of ~0.15 at room temperature,[2] and the maximum quantum efficiency-current–density product achieved at $T = 5$ K is $\eta_{EXT} J = 0.3$ A/cm^2.[1] Even if a consideration is made for incomplete collection of the electroluminescence in the reported results, this appears to be considerably less than that required for lasing in a practical structure (see Sec. III). Finally, the tetracene device of Fig. 1(a) lacks charge and optical confinement, two important requirements for achieving lasing in semiconducting materials.[12] Thus, the report of spectral narrowing in tetracene is remarkable, as it suggests that lasing could be achievable in an optimized structure. The origins of the spectral narrowing must, therefore, be resolved. Our analysis suggests that while lasing in bulk tetracene is unlikely, electrical confinement at interfaces may promote nonlinear effects such as self-focusing, or the formation of an electron-hole plasma. These processes might lead to substantial optical gain, or even lasing in optimized structures.

2. Nonradiative losses in tetracene

For optical characterization, tetracene crystals were grown at atmospheric pressure in argon following the technique of Kloc *et al.*[46] A photograph of a typical crystal is shown in Fig. 8(a); it is ≈10-μm thick and 1-cm long. To determine the effect of nonradiative losses, we measured the relative quantum yield by optically exciting a single crystal with a nitrogen laser. The pump laser generated 1-ns pulses at a wavelength of $\lambda = 337$ nm with a peak energy density of 720 μJ/cm^2 when focused on to a 1-mm-diameter circular spot. Given 90% absorption within the crystal, we estimate that singlet densities as high as 10^{16} cm^{-3} are generated at the highest pump-laser fluence. For a circular pump beam, a cavity is formed between the parallel top and bottom crystal facets. The beam was also shaped in a $\sim 10 \times 0.5$ mm^2 stripe using a cylindrical lens, forming a continuous gain-guided cavity across the length of a crystal with two parallel facets oriented normal to the beam direction. The facet reflectivities in both geometries were ~8%, similar to that in the structure of Ref. 1. The spectra in both orientations were identical, and

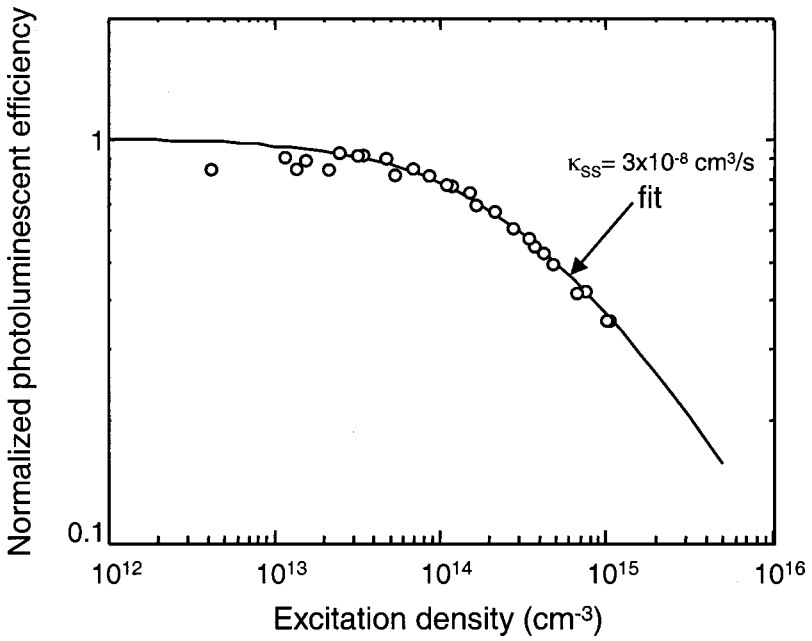

FIG. 9. The normalized quantum yield of tetracene under photoexcitation. Strong singlet-singlet annihilation is observed for densities of photoexcited singlets, $N_S > 10^{15}$ cm^{-3}. The fit to the quantum efficiency yields $\kappa_{SS} = 3 \times 10^{-8}$ cm^3/s, consistent with previous studies of this phenomenon.

as shown in Fig. 8(b), no significant narrowing or threshold in intensity was observed in the photoluminescent spectrum of tetracene for estimated singlet densities of $N_S \leqslant 10^{16}$ cm^{-3}.

The normalized photoluminescent efficiency as a function of N_S is shown in Fig. 9. In agreement with previous studies,[47] the efficiency is found to decrease at high excitation densities. This has been attributed[47] to singlet-singlet annihilation [see Eqs. (2) and (14)], and from a fit to these data (solid line), we find $\kappa_{SS} = 3 \times 10^{-8}$ cm^3/s, also in agreement with previous studies.

The impact of singlet-singlet annihilation-on the optical gain in tetracene is described by the external quantum efficiency-current–density product, calculated from Eqs. (23) and (24). At low temperature we assume that the internal quantum efficiency is limited only by spin statistics [$\xi/(1+\xi) = 0.25$], but at room temperature we also include the photoluminescent efficiency of tetracene[2] ($\eta_{PL} = 0.15$), i.e., in Eq. (15), $\eta_0 = \eta_{PL}\xi/(1+\xi)$. The optical gain is then calculated as a function of singlet density N_S and current density J, as shown in Fig. 10 for a crystal thickness of 10 μm. At inversion densities of $N_S \sim 10^{16}$ cm^{-3}, singlet-singlet annihilation reduces the expected optical gain to $\gamma \sim 0.8$ cm^{-1}. It is likely, therefore, that the lack of spectral narrowing observed in Fig. 8 is due to waveguide and other residual absorption losses exceeding the relatively small

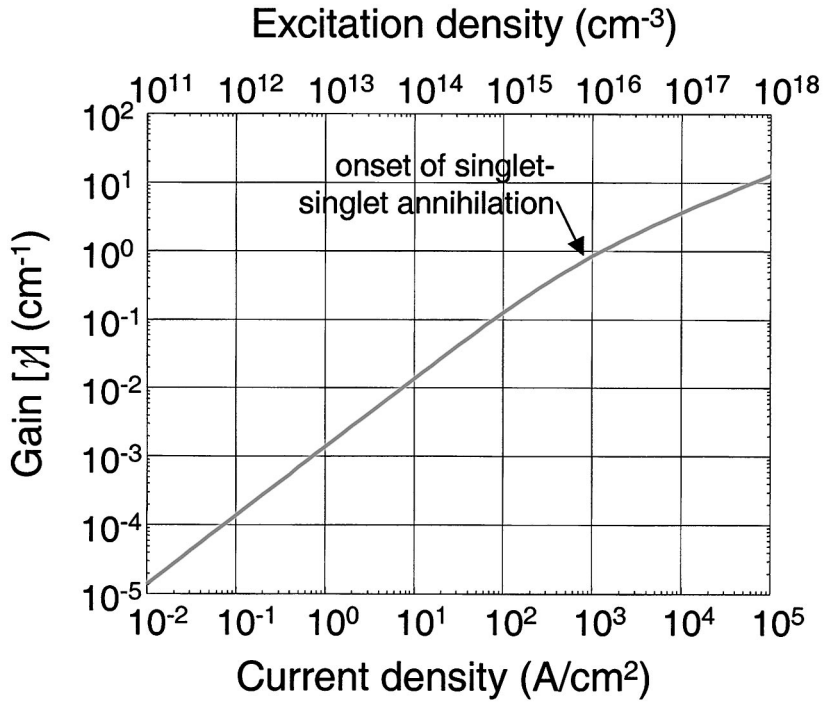

FIG. 10. Calculated optical gain in tetracene at room temperature as a function of applied current density (bottom axis) and photoexcited singlet population (top axis). The crystal thickness is 10 μm and the optical confinement is assumed to approach unity. The inflection is due to the onset of singlet-singlet annihilation. For the maximum pump intensity in Fig. 8(b) the optical gain is only $\gamma = 0.8$ cm^{-1}. This corresponds to an applied current density of $J \sim 1$ kA/cm^2.

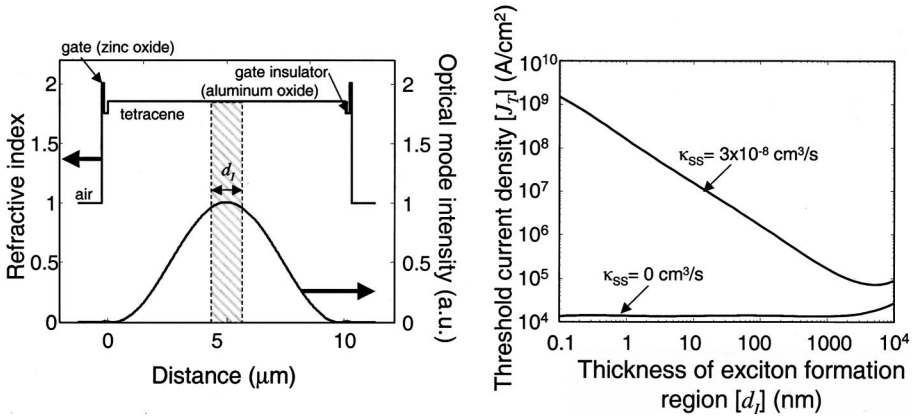

FIG. 11. (a) For a tetracene refractive index of $n=1.85$, optimum optical confinement is achieved for the fundamental mode shown. The corresponding current density at lasing threshold is shown in (b) for low-temperature tetracene. The threshold is calculated with and without the effects of singlet-singlet annihilation. In both cases, however, the current density required for lasing is at least $J=10$ kA/cm^2.

maximum optical gain. For a tetracene crystal of 10 μm thickness, the current density corresponding to an inversion density required for an optical gain of $\gamma \leqslant 1\ \mathrm{cm}^{-1}$ is $J \sim 1000\ \mathrm{A/cm}^2$. Given the expected mirror losses in the device of Schön *et al.*[1] of $\alpha \sim 30\ \mathrm{cm}^{-1}$, the lasing in the bulk tetracene crystal requires at least $J_{\mathrm{TH}} \sim 100\ \mathrm{kA/cm}^2$.

3. Optical confinement and laser physics in bulk tetracene

Figure 10 gives the threshold current, $J_{\mathrm{TH}} \sim 100\ \mathrm{kA/cm}^2$, demonstrating that bulk lasing is unlikely, given the relatively poor charge-carrier mobility of molecular organic crystals. This simple calculation assumes an optical confinement factor $\Gamma=1$ and an exciton formation zone thickness of $d_I=10$ μm. In the structure of Schön *et al.*,[1] the dual thin-film transistor injecting contacts allow both hole and electron currents to be tuned individually, and consequently it is necessary to consider possible differences between the crystal thickness and d_I. To estimate the confinement factor, we calculate the optical modes assuming an electrode (zinc oxide) thickness of 100 nm with a refractive index of 2.0, a gate insulator (aluminum oxide) thickness of 150 nm and refractive index of 1.75, and a tetracene thickness of 10 μm with a refractive index of 1.85. Approximately 55 optical modes are supported in this thick cavity; of these, the lowest-order mode typically has the maximum overlap with the gain region, as shown in Fig. 11(a). Only $\sim$0.01% of this mode is confined within the gate electrodes, the remainder is confined in the gate insulator and tetracene crystal. We estimate that absorption losses in zinc oxide may be as low as 1 cm^{-1}.[11] In any case, the lasing threshold current for this optical mode is determined primarily by the mirror losses; using a length of $L=750$ μm and reflectivity at the organic/air interface of $R \sim 0.08$, we get $\alpha_T = (1/L)\ln(R) \sim 30\ \mathrm{cm}^{-1}$.

In Fig. 11(b), we show the threshold current density for various values of d_I between 0.1 nm and 10 μm. The confinement factor scales approximately linearly with d_I, but singlet-singlet annihilation increases the lasing threshold current for $d_I \ll 1$ μm. The minimum threshold current density is $J_{\mathrm{TH}} \sim 6\times10^4\ \mathrm{A/cm}^2$ for $d_I \sim 5$ μm. This is significantly greater than the reported[1] threshold current density of $J_{\mathrm{TH}} = 500\ \mathrm{A/cm}^2$ at $T=5$ K. Electrical pumping of bulk, intrinsic tetracene, therefore, is very unlikely to be the source of the optical gain observed by Schön *et al.*[1] However, it is possible that singlet-singlet annihilation may be overcome by trapping the excitations [i.e., $D \rightarrow 0$ in Eq. (1)] at crystalline defects.

Crystalline tetracene, like all polyacenes, possesses molecular vacancies that disrupt crystalline order.[17] Since the energy of vacancy formation is expected to be similar to the lattice energy, these vacancies cannot be removed simply by annealing.[17] Vacancies cause a decrease in the polarization energy of surrounding carriers, and hence are expected to act as charge scattering centers.[17] Crystalline dislocations, in contrast, are thermodynamically unstable and may be removed by annealing.[17] Excitons are known to be trapped at dislocations, strain minima, and other inhomogenities in organic crystals, where they may have slow rates of singlet-singlet annihilation.[2,17] Alternatively, in Sec. V A we consider the possibility of electron-hole plasmas, which are not expected to be affected by excitonic processes such as singlet-singlet annihilation. Accordingly, we plot the threshold current density in Fig. 11(b) in the absence of singlet-singlet annihilation. But even in the absence of these nonradiative losses, the threshold current remains high. Indeed, without optical confinement, gain is probably not achievable in intrinsic, bulk tetracene at practical drive current densities.

4. Optical confinement and laser physics at tetracene interfaces

The actual location of the recombination zone in the device of Ref. 1 is unclear. Since the injection efficiencies of both positive and negative carriers are independently tuned by adjusting the gate voltages, a misalignment in charge transport or injection can swing the exciton formation region to either of the tetracene/aluminum oxide interfaces. These interfaces provide two-dimensional carrier confinement, possibly reducing the rate of singlet-singlet annihilation. Furthermore, the high densities of interfacial charge ($\sim 10^{13}\ \mathrm{cm}^{-2}$) (Ref. 1) should locally reduce the refractive index of tetracene, and in Fig. 12(a) we find that a single optical mode may be confined within the high index gate oxide if the tetracene refractive index is reduced to $n_r \sim 1.80$. Thus, rather than causing antiguiding, it is possible that high charge densities at the tetracene interface may help to establish optical confinement near a gate electrode. Because this mode leaks significantly into the organic gain me-

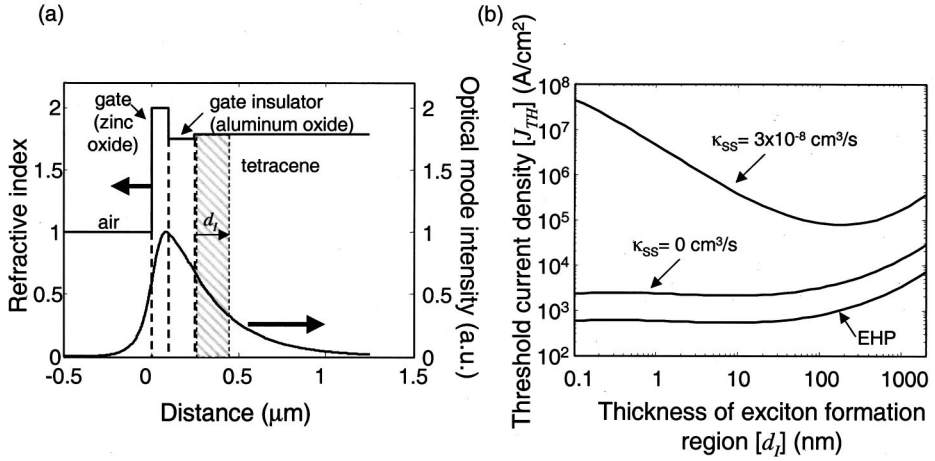

FIG. 12. (a) A leaky mode is supported in the transparent gate electrode for an interfacial tetracene refractive index of $\approx n=1.80$. Optical confinement is superior to that found in Fig. 11, and the corresponding current density at lasing threshold, shown in (b), is thereby reduced. The threshold is calculated with and without the effects of singlet-singlet annihilation, and the current density required for lasing is found to be at least $J_{\mathrm{TH}}=2\ \mathrm{kA/cm^2}$. By assuming the formation of an electron-hole plasma and the absence of both singlet-singlet annihilation and spin-selective radiative recombination, the threshold current density is found to be at least $J_{\mathrm{TH}}=500\ \mathrm{A/cm^2}$, similar to that reported by Schön *et al.* (Ref. 1).

dium, the combination of a higher confinement factor Γ and localized reduction of singlet-singlet annihilation may lower the threshold current density required for lasing. Such a situation is shown in Fig. 12(b), where we have assumed combined mirror and absorption losses of $\alpha_T=60\ \mathrm{cm^{-1}}$.[11] The minimum threshold current density is $J_{\mathrm{TH}}>2\ \mathrm{kA/cm^2}$. Although this result is obtained in the absence of singlet-singlet annihilation, it is too high to explain the spectral narrowing reported in Ref. 1.

If optical confinement at an interface is not provided by the structure itself, then extrinsic effects must be considered. It is possible that the injection transistors are biased into ambipolar operation, i.e., $V_{\mathrm{DS}}\sim 2V_G$, such as more recently reported for the light-emitting thin-film transistor of Schön *et al.*[48] Under these conditions, an approximately triangular interfacial charge distribution is formed. These polarons interact with the optical field of an electromagnetic wave, reducing the dielectric constant if the optical field has a higher frequency ν than that of the polaron resonance, ν_0.[45] In this case, the resultant change in the refractive index n_r is given by[33]

$$\delta n_r=-\frac{1}{16\pi^2}\frac{nq^2}{n_r^2\varepsilon_0 m_{\mathrm{eff}}m_0}\frac{\nu/\nu_0-1}{(\Delta\nu/2)^2+(\nu-\nu_0)^2}, \quad (26)$$

where n is the carrier density, m_{eff} is the effective mass of carriers in the organic crystal, m_0 is the free-electron mass, and $\Delta\nu$ is the half-width of the polaron absorption.

The change in refractive index described in Eq. (26) depends on intermolecular overlap, and is much stronger in organic crystals than in thin amorphous films. This is because m_{eff} is inversely proportional to the energy bandwidth. But the effect is expected to be weaker in organic crystals than in some conventional inorganic semiconductors, where it may be used to tune the frequency of semiconductor lasers. For example, the effective mass of holes in anthracene has been measured to be between $10m_0$ and $20m_0$ using cyclotron resonance.[49,50] Schön *et al.*[51] have measured the effective mass of holes in a two-dimensional gas in tetracene to be $(1.3\pm 0.3)m_0$. Even this latter value is $\sim$20 times higher than, for example, GaAs, where $m_{\mathrm{eff}}=0.067$ (electrons) and $m_{\mathrm{eff}}=0.34$ (holes). Assuming that the effective masses of electrons and holes in tetracene are roughly similar, the constant of proportionality between δn_r and the carrier density n in tetracene is $\approx -2\times 10^{-22}\ \mathrm{cm^3}$ at $\lambda=570$ nm; an effect significantly reduced relative to that found in inorganic semiconductor lasers.

In a tetracene TFT, the interfacial charge may approach $10^{13}\ \mathrm{cm^{-2}}$ at $V_G\sim 50$ V, enough to reduce the refractive index by as much as 10% in the interfacial layer [cf. Eq. (26)]. Thus, under ambipolar operation, which may also occur in Ref. 1 , the interfacial charge density will form a weak optical waveguide in the channel. However, the interfacial layer is extremely thin and changes in its refractive index are not expected to significantly alter the overall optical confinement in the structure.

V. DISCUSSION

A. High excitation effects

In Sec. IV B, it was determined that there is insufficient structural, electrical, and optical confinement in the tetracene device of Ref. 1 to explain the observed spectral narrowing. We now consider two other potential extrinsic effects that may contribute to this phenomenon. The first effect is the formation of an electron-hole plasma[52] (EHP), which is caused by the extremely high densities of charges and excitons created by electrical confinement near an interface. The critical density of electron-hole pairs, n_p^c, required for formation of an EHP is given approximately by

$$a_B^3 n_p^c \approx 1, \quad (27)$$

where a_B is the Bohr radius of the charge pairs. For organic materials, the exciton is often no larger than the molecular diameter.

At $V_G \sim 50$ V, the interfacial charge density in the exciton formation zone is 10^{13} cm^{-2}, and we estimate that the density of charges may approach the density of molecular sites. Under these conditions, free carriers screen the Coulomb interactions within the excitons themselves.[52] In addition, phase-space filling of the bands at the interface excludes some electronic states required to complete excitonic wave functions.[52] Phase-space filling is generally marked by a relative increase in luminescence from the blue, unfilled, transitions in the vibronic manifold and it may account for the appearance of gain from the 1-0 transition in tetracene.[1] Both, screening by free carriers and phase-space filling prevent exciton formation, and lead to the creation of an EHP.[52]

One consequence of the formation of an EHP is the disappearance of the quasiparticle nature of discrete excitons. This, in turn, eliminates many excitonic processes such as singlet-singlet annihilation and spin-selective radiative recombination in favor of direct band-to-band recombination at the interface, or other regions (such as that surrounding a defect) where excitons and carriers would localize at high densities. Indeed, the absence of laser emission at even the highest exciton densities generated by optical pumping [see Fig. 8(b), where $n \ll n_p^c$] suggests that free carriers rather than excitons are the source of the spectral narrowing in Ref. 1.

We expect that singlet-singlet annihilation will be replaced by nonradiative Auger processes in the EHP, but the latter loss mechanisms may have a lower probability due to phase-space filling. Thus, in Fig. 12(b), we plot the expected threshold current density given that $\kappa_{SS}=0$, and that the ratio of radiative states to free electrons is equal to unity, characteristic of free carriers occupying bandlike states. The minimum threshold current density for lasing is found to closely approach that reported by Schön *et al.*,[1] i.e., $J_{TH} = 500$ Å/cm^2.

The effects of the high-density EHP may be reinforced by optical confinement introduced by a second nonlinear effect: self-focusing due to intensity-dependent saturation of the anomalous dispersion.[53] To estimate the strength of this effect, we note that the refractive index n_r in a homogeneously broadened system such as tetracene is related to the optical gain by

$$\delta n_r \approx -\frac{n_r}{k}\frac{\omega_0-\omega}{\Delta\omega}\frac{\gamma}{1+I/I_S},$$

$$\delta n_r(I) \approx \frac{n_r\gamma}{k}\frac{\omega_0-\omega}{\Delta\omega} I/I_S, \tag{28}$$

where ω_0 is the angular frequency of the radiative transition of tetracene, $\Delta\omega$ is the spectral width, and I_S is the saturation optical intensity[33]

$$I_S = \frac{8\pi n_r^2 hc^2 \Delta\lambda}{\eta_{PL}\lambda_0^5}. \tag{29}$$

Thus, the refractive index increases with the laser intensity, and given sufficient light intensity, tetracene spontaneous emission may form its own waveguide.

In conventional semiconductor lasers, saturation dependent self-focusing below threshold is usually overwhelmed by the plasma effect [see Eq. (26)]. The lack of carrier confinement in the tetracene bulk should minimize antiguiding because the carrier density within the crystal may be quite uniform. In any case, as discussed earlier, the plasma effect is expected to be weaker in organic materials than in conventional semiconductor laser materials.

From Eq. (29), the saturation intensity in tetracene is ≈ 3.3 MW/cm^{-2}, well above the expected intensity within the laser cavity if the excitons are uniformly distributed. But the saturation intensity may be realized at dislocations within the tetracene crystal. For example, if excitons are trapped within dislocations of area $\sim 10 \times 100$ nm^2, the saturation power is reduced to 33 μW. If optical confinement, $\Gamma \rightarrow 0.1$, occurs within an exciton formation region of thickness $d_I \sim 10$ nm, then the current density at the lasing threshold is $\approx J_{TH} = 1000$ A/cm^2.

The agreement of the expected threshold current with the result of Schön *et al.*[1] suggests that high-density EHP's and optical confinement aided, in part, by self-focusing at defects or at the strained Al_2O_3/tetracene interface, may be the source of the reported gain and spectral narrowing. However, we stress that while substantial optical gain is reported in these structures, lasing in tetracene has not yet been convincingly achieved, as noted in Sec. IV. In any case, further investigation of the possible role of both self-focusing and EHP's in organic semiconductor crystals is needed to fully understand the results of Ref. 1.

B. Crystalline versus amorphous organic lasers

Both crystalline and amorphous organic devices suffer from nonradiative losses. The physical deterioration of the amorphous CBP/BCP device in Sec. IV A limits the maximum quantum efficiency-current density product to $\eta_{EXT}J = 0.06$ A/cm^2. It is likely that this can be corrected by using a combination of more stable materials. A reasonable estimate is $\eta_{EXT}=0.02$ at $J=40$ A/cm^2, giving $\eta_{EXT}J \sim 1$ A/cm^2, corresponding to a peak output power of 1 W/cm^2, and similar to that required for lasing in an optimized structure (i.e., where $\alpha_T = 1$ cm^{-1}). The maximum quantum efficiency-current density product of the crystalline tetracene device is similar, at $\eta_{EXT}J = 0.3$ A/cm^2. Consequently, it is not immediately obvious that crystalline materials offer any significant advantages over amorphous organic semiconductors as lasing materials, and considering the processing advantages of amorphous materials, electrically pumped amorphous materials may deserve further attention.

However, as noted in Sec. V A, an intriguing possibility raised by the work of Schön *et al.*[1] is the formation of electron-hole plasmas in crystalline materials under sufficient pumping densities. As described in Sec. IV, it is diffi-

cult to account for the observation of spectral narrowing in tetracene without explaining the apparent absence of singlet-singlet annihilation. Phase-space filling in an EHP may reduce this loss pathway, and ionization of excitons will eliminate the formation of nonradiative triplet states. This appears to be the most likely explanation for the results of Schön *et al.*[1] Although both crystalline and amorphous materials could conceivably host an EHP, the excitation strength required for its formation is related to the size of an exciton by Eq. (27). Amorphous materials possess the most highly localized Frenkel excitons that may ultimately discourage the formation of an EHP.

In the absence of a technique for minimizing nonradiative losses in amorphous materials, a potential thin-film lasing structure must be designed for very low cavity losses, i.e., $\alpha_T \rightarrow 1\ \mathrm{cm}^{-1}$. Thicker, doped transport layers can be used to separate the luminescent region from absorptive injection contacts.[54] Or, the transport layers in a double heterostructure might be fabricated from crystalline or polycrystalline materials for improved charge transport mobility. Injection-limited transport can be overcome by thin-film transistor injection contacts such as those employed by Schön *et al.*[1]

But the fabrication of such a cavity is challenging to current organic technologies, and in any case, it is possible that polaron absorption will increase at high current densities.[11] Thus, alternative strategies may need to be developed for an all-organic, amorphous, electrically pumped laser. For example, an optimal threshold current might be obtained by separating the pump and gain regions altogether, using an OLED to optically pump a low loss organic laser. This approach minimizes nonradiative losses and increases flexibility in the design of the laser cavity. Given current OLED quantum efficiency-current density products, some focusing of the pump will be required by the structure. But the fabrication of a ''flashlamp'' organic laser would be a significant step towards a practical, amorphous, organic laser.

VI. CONCLUSION

We conclude with the following observations.

(i) Suitable lasing materials may be recognized by a quantum efficiency that is relatively independent of current density and electric field. The external quantum efficiency-current–density product must be at least $\eta_{\mathrm{EXT}} J = 5\ \mathrm{A/cm}^2$.

(ii) Although OLED's are highly efficient at low current densities, increases in nonradiative losses with excitation strength are a serious obstacle to obtaining an electrically pumped laser. Crystalline materials are particularly susceptible to nonradiative losses caused by bimolecular reactions between singlet excitons. Losses in amorphous organic materials are caused by high densities of triplets and polarons.

(iii) We have been unable to reconcile the characteristics of the device in Ref. 1 with the known properties of tetracene, notably its excitonic losses. Furthermore, lasing has not been convincingly demonstrated in the device reported by Schon *et al.* Nevertheless, one possibility for reducing losses is operation with extreme densities of charge in the exciton formation zone, which may result in the formation of an electron-hole plasma, thereby avoiding excitonic loss processes such as singlet-singlet annihilation and spin-selective radiative recombination.

(iv) At present, it is unclear whether an electron-hole plasma can be formed in an organic material. If nonradiative losses at high excitation strengths cannot be avoided in thin-film materials, then a significant step toward an electrically pumped laser may be a hybrid flashlamp structure, with an electroluminescent pump separated from an optical gain region. This technique[55,56] can isolate the gain region from electrically induced losses.

ACKNOWLEDGMENTS

This work was supported by Universal Display Corporation, the Air Force Office of Scientific Research, and the National Science Foundation MRSEC program. We thank Professor Chihaya Adachi for his assistance in constructing the tetracene crystal growth reactor, and Dr. J. H. Schön for providing unpublished details concerning the structure and performance of the tetracene device.

*Present address: Department of Electrical Engineering and Computer Science, Massachusetts Institute of Technology, Cambridge, MA 02139.

[1] J. H. Schön, C. Kloc, A. Dodabalapur, and B. Batlogg, Science **289**, 599 (2000).
[2] S. V. Frolov, C. Kloc, J. H. Schön, and B. Batlogg, Chem. Phys. Lett. **334**, 65 (2001).
[3] V. G. Kozlov, V. Bulovic, P. E. Burrows, and S. R. Forrest, Nature (London) **389**, 362 (1997).
[4] N. Tessler, G. Denton, and R. Friend, Nature (London) **382**, 695 (1996).
[5] F. Hide, M. Diaz-Garcia, B. Schwartz, M. Andersson, Q. Pei, and A. Heeger, Science **273**, 1833 (1996).
[6] S. Frolov, M. Ozaki, W. Gellermann, Z. Vardeny, and K. Yoshino, Jpn. J. Appl. Phys., Part 2 **35**, L1371 (1996).
[7] H. Brouwer, V. Krasnikov, A. Hilberer, and G. Hadziioannou, Adv. Mater. **8**, 935 (1996).
[8] M. Berggren, A. Dodabalapur, R. E. Slusher, and Z. Bao, Nature (London) **389**, 466 (1997).
[9] V. G. Kozlov *et al.*, J. Appl. Phys. **84**, 4096 (1998).
[10] V. G. Kozlov, P. E. Burrows, G. Parthasarathy, and S. R. Forrest, Appl. Phys. Lett. **74**, 1057 (1999).
[11] V. G. Kozlov *et al.*, IEEE J. Quantum Electron. **36**, 18 (2000).
[12] L. A. Coldren and S. W. Corzine, *Diode Lasers and Photonic Integrated Circuits* (Wiley, New York, 1995).
[13] C. Adachi, M. A. Baldo, M. E. Thompson, and S. R. Forrest, J. Appl. Phys. **90**, 5048 (2001).
[14] D. J. Pinner, N. Tessler, and R. H. Friend, Synth. Met. **102**, 1108 (1999).
[15] N. Tessler, N. T. Harrison, and R. H. Friend, Adv. Mater. **10**, 64 (1998).
[16] N. Tessler *et al.*, Synth. Met. **115**, 57 (2000).
[17] M. Pope and C. Swenberg, *Electronic Processes in Organic Crys-*

tals (Oxford University Press, Oxford, 1982).
[18] T. Förster, Discuss. Faraday Soc. **27**, 7 (1959).
[19] For example, typical singlet and triplet energy levels can be obtained by modeling the exciton with a hydrogenic wave function.
[20] S. R. Forrest, Chem. Rev. **97**, 1793 (1997).
[21] I. Sokolik, R. Priestley, A. D. Walser, R. Dorsinville, and C. W. Tang, Appl. Phys. Lett. **69**, 4168 (1996).
[22] M. A. Lampert and P. Mark, *Current Injection in Solids* (Academic, New York, 1970).
[23] M. A. Baldo and S. R. Forrest, Phys. Rev. B **64**, 085201 (2001).
[24] C. W. Tang and S. A. VanSlyke, Appl. Phys. Lett. **11**, 913 (1987).
[25] M. A. Baldo, M. E. Thompson, and S. R. Forrest, Nature (London) **403**, 750 (2000).
[26] M. A. Baldo, D. F. O'Brien, M. E. Thompson, and S. R. Forrest, Phys. Rev. B **60**, 14 422 (1999).
[27] M. A. Baldo, C. Adachi, and S. R. Forrest, Phys. Rev. B **62**, 10 967 (2000).
[28] W. Stampor, J. Kalinowski, P. D. Marco, and V. Fattori, Appl. Phys. Lett. **70**, 1935 (1997).
[29] I. G. Hill, A. Kahn, Z. G. Soos, and R. A. Pascal, Chem. Phys. Lett. **327**, 181 (2000).
[30] J. Kalinowski, N. Camaioni, P. Di Marco, V. Fattori, and A. Martelli, Appl. Phys. Lett. **72**, 513 (1998).
[31] R. R. Chance, A. Prock, and R. Sibley, Adv. Chem. Phys. **37**, 1 (1978).
[32] V. Bulovic, V. B. Khalfin, G. Gu, P. E. Burrows, D. Z. Garbuzov, and S. R. Forrest, Phys. Rev. B **58**, 3730 (1998).
[33] A. Yariv, *Optical Electronics* (Saunders College, Philadelphia, 1991).
[34] DCM2 is [2-methyl-6-[2-(2,3,6,7-tetrahydro-1H,5H-benzo[ij]quinolizin-9-yl)ethenyl]-4H-pyran-4-ylidene] propanedinitrile.
[35] B. W. D'Andrade, M. A. Baldo, C. Adachi, J. Brooks, M. E. Thompson, and S. R. Forrest, Appl. Phys. Lett. **79**, 1045 (2001).
[36] I. G. Hill and A. Kahn, J. Appl. Phys. **86**, 4515 (1999).
[37] D. F. O'Brien, M. A. Baldo, M. E. Thompson, and S. R. Forrest, Appl. Phys. Lett. **74**, 442 (1999).
[38] S. Tokito, H. Tanaka, A. Okada, and Y. Taga, Appl. Phys. Lett. **69**, 878 (1996).
[39] S. Tokito, H. Tanaka, A. Okada, and Y. Taga, IEEE Trans. Electron Devices **44**, 1239 (1997).
[40] G. Kaye and T. Laby, *Tables of Physical and Chemical Constants* (Longman, Essex, England, 1995).
[41] P. E. Burrows *et al.*, J. Appl. Phys. **79**, 7991 (1996).
[42] Detector supplied by Molectron, 7470 SW Bridgeport Rd., Portland, OR 97224.
[43] T. Tsutsui *et al.*, Jpn. J. Appl. Phys., Part 2 **38**, L1502 (1999).
[44] J. H. Schön (private communication).
[45] G. H. B. Thompson, *The Physics of Semiconductor Laser Devices* (Wiley, Chichester, 1980).
[46] C. Kloc, P. Simpkins, T. Siegrist, and R. Laudise, J. Cryst. Growth **182**, 416 (1997).
[47] A. J. Campillo, R. C. Hyer, S. L. Shapiro, and C. E. Swenberg, Chem. Phys. Lett. **48**, 495 (1977).
[48] J. H. Schön, A. Dodabalapur, C. Kloc, and B. Batlogg, Science **290**, 963 (2000).
[49] D. M. Burland, Phys. Rev. Lett. **33**, 833 (1974).
[50] D. M. Burland and U. Konzelmann, J. Chem. Phys. **67**, 319 (1977).
[51] J. H. Schön, C. Kloc, and B. Batlogg, Science **288**, 2338 (2000).
[52] C. F. Klingshirn, *Semiconductor Optics* (Springer-Verlag, Berlin, 1995).
[53] J. E. Bjorkholm and A. Ashkin, Phys. Rev. Lett. **32**, 129 (1974).
[54] G. Parthasarthy, C. Shen, A. Kahn, and S. R. Forrest, J. Appl. Phys. **89**, 4986 (2001).
[55] M. Shtein, H. F. Gossenberger, J. B. Benziger, and S. R. Forrest, J. Appl. Phys. **89**, 1470 (2001).
[56] M. A. Baldo *et al.*, Adv. Mater. **10**, 1505 (1998).
[57] H. Ishii, K. Sugiyama, E. Ito, and K. Seki, Adv. Mater. **11**, 605 (1999).
[58] B. Chen and S. Liu, Synth. Met. **91**, 169 (1997).